Research Article

Evaluating the Relationship between Reservoir Level Changes and Earthquake Damage Responses of High Arch Dams: A 3D Numerical Study of Ermenek Arch Dam (220 m) in Turkey

Murat Cavuslu (ORCID)

Department of Civil Engineering, Zonguldak Bulent Ecevit University, 67100 Zonguldak, Turkey

Correspondence should be addressed to Murat Cavuslu; murat.cavusli@beun.edu.tr

Examining the earthquake behaviors of important water structures such as arch dams is of great importance for the future and safety of these structures. Besides, different reservoir heights, which occur as a result of different seasonal precipitation, can cause great losses in the structural behavior of arch dams. For this reason, in this study, the effects of various reservoir water heights on the earthquake behavior of arch dams are evaluated by considering a creep material model. Ermenek dam, one of the highest dams in Turkey, is chosen for the 3D (3D) numerical analyses. This dam has 4 different gallery spaces in its body and it has a body height of 220 m. While creating a 3D finite-different model of the dam, the creep material models are utilized for the concrete and foundation sections. For the 3D earthquake analyses, free-field and quiet nonreflecting boundary conditions (BCs) are defined to the boundaries of the model. Besides, fix BCs are added to the base of the dam. While creating the gallery spaces of the dam, the original dam project is taken into consideration, and attention is paid to creating the oval geometry of the gallery spaces following the project. For earthquake analyses, 4 different water levels (25 m, 85 m, 150 m, and 200 m) are considered, and hydrostatic forces and water table are used while generating the reservoir water. Furthermore, a total of 18 different strong ground motions are used in the earthquake analyses to examine the earthquake behavior of the dam. According to the earthquake analyses, it is concluded that different reservoir heights have great effects on the earthquake behavior of the Ermenek dam. Moreover, it has been observed that the height of the reservoir water causes significant earthquake stress and displacement differences around the gallery spaces of the dam.

1. Introduction

Water is vital to the survival and health of humanity. Many methods have been developed to store water from past to present, and one of the most important of these methods is the construction of dams. Dams are very important to water structures that allow the accumulation of water for people. Recently, many types of dams are being built around the world and one of these dam types is the arch dam. Arch dams have oval geometry and are built in valleys where the water level is high. Since different water heights occur in arch dams in each season, it is of great importance to examine the effects of water heights on the creep and earthquake behavior of these dams. Due to arch dams are very important for the continuation of humanity and have a huge body volume,

they have been the focus of attention of researchers from past to present. Ahmadi et al. proposed a crack model for arch dams. Interaction condition was defined between the dam and reservoir water. Moreover, the mechanical properties of contraction joints were determined by using experimental tests [1]. Akkose et al. examined the reservoir water effects on earthquake behavior of arch dams considering the Drucker–Prager model and a total of 5 various water levels. It was deduced that after a certain water level is reached, the crest displacements of the dam and the arch stresses on the dam body increase significantly [2]. Amina et al. studied the modal behavior of arch dams considering the fluid-structure interaction. According to numerical analyses, it was seen that the natural frequencies of the dam–massless foundation model are well lower for without

water situation of the dam model [3]. Feng et al. examined the safety procedures of arch dams utilizing safety factors (k1, k2, and k3) [4]. Jin et al. assessed the effects of foundation models on the earthquake behavior of arch dams. It was deduced that the rock classes and faults influence the dynamical behavior of arch dams [5]. Li et al. proposed a new method for the material parameter inversion of the arch dams and dam foundations [6]. Lotfi and Espandar investigated the earthquake analyses of arch dams using two crack techniques. According to the analysis results of four various cases, critical cracks, and principal stress (PS) values were obtained on up sections of the dam body [7]. Lotfi investigated the direct frequency domain analyses of concrete arch dams and the effects of canyon shape on the response of the dam were determined using FE-(FE-HE)-BE techniques [8]. Ma et al. examined the stability analyses of arch dams considering 3D modeling and overload factors of crack initiation [9]. Malla and Wieland examined the horizontal crack behavior of arch-gravity dams considering the daily temperature changes. It was observed that a horizontal crack first appeared along the downstream wall of the upper gallery of an arch-gravity dam after 25 years of operation [10]. Mirzabozorg et al. evaluated the earthquake behavior of arch dams considering massed foundation effects. It was seen that modeling of the dam foundation ensures the significant overestimation of the dynamical response of the arch dams [11]. Moradloo et al. investigated the damage behavior of arch dams utilizing underwater explosions. It was concluded that tensile damage is the main cause of arch dam damage [12]. Nasserzare et al. assessed the structural performances of arch dams considering an algorithm [13]. Li et al. assessed the structural behavior of arch dams taking into account diurnal temperature variation and the sub-model analysis method. It was seen that the sub-model analysis method is an important alternative approach to studying the changing laws of the temperature field of arch dams [14]. Xu et al. investigated the stochastic earthquake response of an arch dam. It was observed that cracking first occurs on the base surface near the upstream face [15]. Pan et al. examined the earthquake effects of initial stresses on the 3D dynamic behavior of arch dams. It was seen that the initial stress is very important for the structural response of high arch dams subjected to underwater explosions [16]. Pereira et al. monitored the dynamical behavior of arch dams during the first filling of the reservoir. It was seen that the first 6 vibration modes are close to each other for ambient vibration, forced vibration, and numerical modeling [17]. Aftabi Sani and Lotfi assessed the dynamical behavior of arch dams considering the ideal-coupled modal approach. Reservoir water was modeled using fluid finite elements and fluid-hyper elements [18]. Such as these studies, many researchers pioneered to examine of the structural behavior of arch dams [19–32]. Moreover, the stress verifications of large concrete existing dams were performed considering the comparison of two earthquake Italian codes. Reservoir water was created by applying "added masses" to the water-holding surfaces of the dam and their value is acquired by using the Westergaard hydrodynamic overpressures [37]. In a study, the effects of quasi-static seasonal loadings on the structural response of concrete dams were examined in detail and it was suggested that the bathymetry near the dam's wet surface should be considered when creating the reservoir geometry [38]. Then, for concrete dams, the bearable maximum earthquake action was examined using finite element simulations and a multipurpose code [39]. As seen from these studies, there are no studies about the effects of reservoir water levels on the earthquake behavior of high arch dams. Besides, it is seen that researchers have not examined the effects of 3D oval gallery spaces on earthquake and crack behaviors of arch dams. For this reason, this study will shed light on both the literature and future studies.

2. Scope of the Study

In this study, the effects of different reservoir levels and various gallery spaces on the earthquake behavior of arch dams are discussed in detail. First, the Ermenek dam is modeled in 3D using FLAC3D software. While creating the dam model, the finite-difference (FD) method is utilized. The Burgers–Mohr material model is considered for the dam concrete and dam foundation. This material model was not utilized to examine the earthquake response of the arch dams. However, this material model was developed to reveal and study the failure and time-dependent creep behavior of materials such as rock or concrete. For this reason, one of the aims of this study is to reveal the effects of this material model on the earthquake behavior of arch dams. Then, free-field and quiet nonreflecting BCs are defined for the dam's boundaries. In the literature, these nonreflecting BCs were not considered in the earthquake analyses of the arch dams. Another aim of this study is to determine the earthquake effects of these BCs on the earthquake behavior of the arch dams. Reservoir water is modeled using both the water table and water pressures. Ermenek dam has 4 different gallery spaces and these gallery spaces have oval geometry. These oval geometry gallery spaces are modeled in 3D following the dam project. A total of 4 different reservoir water levels are used during earthquake analyses. These reservoir levels correspond to the gallery spaces of the dam, and in this study, the effects of different reservoir water levels around the gallery spaces of arch dams are evaluated in detail. The most important aim of this study is to reveal the earthquake effects of various reservoir water levels on the 3D earthquake response of the arch dams. For this aim, a total of 18 different earthquakes are used for the earthquake analyses of the Ermenek dam. These earthquakes are important ground motions that have occurred in different parts of the world. According to 18 different earthquake analyses, it is concluded that different reservoir water levels have great effects on the earthquake behavior of arch dams. Besides, it is observed that different water levels created various earthquake cracks, critical principal stresses (PSes), and important displacements around gallery spaces. This study makes great contributions to the literature on the effects of both reservoir water levels and various 3D gallery spaces on the earthquake behavior of arch dams.

3. Free-Field and Quiet Nonreflecting Boundary Conditions (BCs)

Earthquake waves are damped from back reflection as they travel through a structure. If we do not realistically model the earthquake waves in the numerical modeling of the structures, accurate earthquake results cannot be obtained [34]. For this reason, in earthquake numerical analyzes, attention should be paid to preventing the earthquake waves from being reflected into the structure. For this aim, special earthquake BCs are utilized during the earthquake analysis of arch dams in this study. In the FLAC3D program, many BCs have been derived for the solution of geotechnical problems [34]. These BCs vary according to the environment in which the structure is located and the load it contacts. There are nonreflecting BCs specially produced for earthquake analysis of structures in the FLAC3D program [34]. These BCs ensure that the earthquake waves do not reflect inside the structure and allow us to obtain more accurate earthquake results [33]. The earthquake boundaries of the Ermenek arch dam modeled using the FLAC3D program are shown in Figure 1. According to Figure 1, earthquake boundaries are defined for the lateral and lower boundaries of the foundation section of the arch dam. Free-field boundary (FFB) conditions are defined to the lateral boundaries of the foundation section and quiet boundary (QB) conditions are defined to the bottom section of the foundation. In this way, the reflection of earthquake waves back in the model is prevented and the results of the earthquake analysis are ensured to be accurate and precise [34].

The FFB condition should be placed to the side boundaries to minimize wave reflections (Figure 1). The FFB condition is defined in the following formulation:

$$F_x = -\rho C_p \left(v_x^m - v_x^{ff} \right) A + F_x^{ff},$$
$$F_y = -\rho C_s \left(v_y^m - v_y^{ff} \right) A + F_y^{ff}, \quad (1)$$
$$F_z = -\rho C_p \left(v_z^m - v_z^{ff} \right) A + F_z^{ff}.$$

In equation (1), ρ: the density, C_p: speed of p-wave, C_s: speed of s-wave, A: area, v_x^m: x-velocity in the grid, v_y^m: y-velocity in the grid, v_z^m: z-velocity in the grid, v_x^{ff}: x velocity in the side, v_y^{ff}: y velocity in the side, v_z^{ff}: z velocity in the side, F_x^{ff}: FF force for σ_{xx}^{ff} stresses, F_y^{ff}: FF force for σ_{xy}^{ff} stresses, and F_z^{ff}: FF force for σ_{xz}^{ff} stresses [34]. Furthermore, the viscous quiet BC should be used in the earthquake analyses of arch dams together with FF BCs. In quiet BC, the earthquake dashpots are considered [34] and the normal and shear earthquake dashpots are calculated as follows:

$$t_n = -\rho C_p v_n,$$
$$t_s = -\rho C_s v_s. \quad (2)$$

In equation (2), v_n and v_s: the normal and shear components for velocity, ρ: density, and C_p and C_s: p and s waves [34].

4. General Information about Ermenek Arch Dam

Ermenek dam, one of the many high dams in the world and the second-highest dam in Turkey, is a thin concrete arch dam with a double curvature asymmetric structure. This dam, which was built in Turkey-Karaman, started to be built in 2002 and was completed in 2009. The body thickness varies along with the height and is 7 m at the crest and 25 m at the lowest part. The dam was built in a very deep and narrow valley. The body width is 150 m in the upper part and less than 5 m in the lower part. The height of the dam is 210 m and the crest length is 123 m [33]. The reservoir volume is 4582 hm³ and the reservoir area is 58.74 km². Its electricity generation capacity is 1047.86 Wh per year. The dam, which was built to generate energy, was built on the Göksu river within the borders of Karaman province in Turkey [33]. The mechanical properties of the Ermenek arch dam are presented in Table 1. Moreover, the general view of the dam is shown in Figure 2.

5. 3D Finite-Difference Modelling of Ermenek Dam

In this study, the earthquake damage performances of high arch dams are investigated by including gallery spaces. For this purpose, the Ermenek arch dam (220 m) is chosen for numerical analyses and the dam is modeled as 3D according to the original project. The modeling processes of the dam are performed using special fish functions developed for the FLAC3D software. There are 4 different gallery spaces with oval geometry inside the dam body and gallery spaces are modeled before the dam body is built. The locations of the galleries are shown in Figure 3. The lengths of gallery spaces are different from each other. The length of gallery 1 is 122 m, and the lengths of gallery 2 and gallery 3 are 79 m and 54 m, respectively. Besides, gallery 4 has a length of 28 m. Before the dam body is created, gallery spaces are constituted, and then concrete material is formed around the gallery spaces. The 3D model of the dam body is shown in Figure 4 in detail. FLAC3D software recommends researchers use both free-field and quiet BCs for earthquake analyses of the arch dams. For this reason, nonreflecting BCs (free-field and quiet) are used to prevent earthquake accelerations from being reflected in the 3D FD model of the dam. These BCs have never been used in the past to assess the earthquake behavior of concrete arch dams. Quiet nonreflecting BC was developed by Lysmer and Kuhlemeyer in 1969 and it is based on using earthquake dashpots at x (normal) and y (shear) directions of special boundaries of the 3D model. Moreover, it is very effective for absorbing earthquake waves that approached the boundary at angles of incidence greater than 30°. In this study, quiet (viscous) BC is practiced to lateral boundaries of the 3D model as seen in Figure 4. Then, the free-field BC is considered for the lateral surfaces of the 3D model (Figure 4). The lateral surfaces of the main grid are coupled to the free-field grid by using viscous dashpots and the unbalanced forces from the free-field grid are applied to the
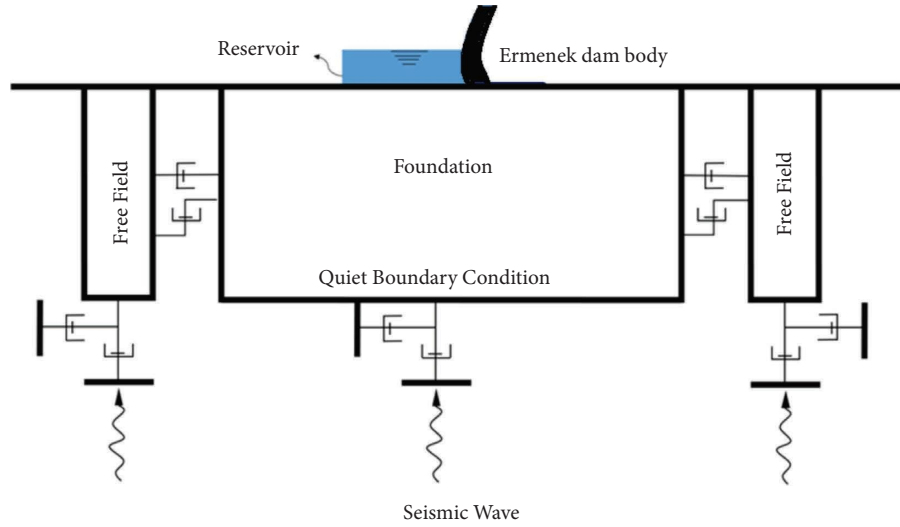
FIGURE 1: Boundaries of the Ermenek arch dam [34].

TABLE 1: Material properties of Ermenek arch dam [33].

Material	E (GPa)	Poisson's ratio	Density (kg/m^3)
Concrete	32	0.24	2615
Rock	22	0.19	2764

main-grid boundary [34]. In free-field earthquake BC, earthquake waves that propagate upward do not break down at the main surfaces. If the grid point is uniform, the earthquake dashpots are not considered due to the free field surface performs the same motion as the main grid [34]. The free-field BC model contains a one-dimensional column at unit width. The free field's height equals the lateral surface's length [34]. Thanks to the nonreflecting BC, the earthquake accelerations circulating in the dam model are prevented from being reflected from the dam boundary [34]. In this study, the hysteretic damping sigmoidal (sig3) model is used for the damping ratios of foundation and concrete. The dynamic characteristics of these materials are governed by two sets of modulus reduction factor (G/Gmax) of the foundation and concrete and damping ratio (λ). The most suitable mesh width is selected for the 3D model of the dam and there is a total of 2876341 volumes in the dam model. Special time definitions are performed for creep analyses. For example, a 10-year time definition is made for the 10-year failure behavior of the dam using special fish functions. While performing creep and earthquake analyses, the program gave errors many times and the dam model is calibrated many times.

To model the interaction condition between discrete surfaces, interface elements are defined between the dam-reservoir water foundation in the normal and shear directions. These interface elements are defined on each nodal point between discrete surfaces. Thanks to the interface elements, a realistic interaction condition is provided between the discrete surfaces. The numerical values of the interface elements in the normal and shear directions defined between the discrete surfaces are 10^8 Pa/m [40]. Interface elements defined between discrete surfaces are shown

in Figure 3. After the dam body is formed, reservoir water is created using both hydrostatic pressure and water table. To model the reservoir water, "added masses" have been applied to the nodal points of the dams' upstream surfaces. Their value is acquired by taking into account the Westergaard hydrodynamic overpressures [37]. Besides, the water table is used to provide the magnitude of water pressure in each FLAC zone [34]. Water loads (added masses) and water table are shown in Figure 5.

The foundation section of the dam is generated by extending the dam body towards the sides and the bottom. The foundation is extended to the sides and the bottom by the height of the dam. Furthermore, the foundation is extended by 2 times the dam height towards the upstream and downstream sides. The Burgers–Mohr material model is used for the foundation material and concrete material of the dam body. The Burgers–Mohr material model has never been used in the past for the creep and earthquake analysis of concrete arch dams. The 3D FD model of the dam is shown in Figure 4 in detail.

Random mesh spaces should not be used when examining the earthquake analyzes of arch dams, and thanks to the Burgers–Mohr material model, the optimum mesh spacing that can be used for arch dam body has been found. Moreover, thanks to the Burgers–Mohr material model, a viscoplastic model in FLAC3D is characterized by a visco-elastoplastic deviatoric behavior and an elastoplastic volumetric behavior [34]. The viscoelastic and viscoplastic strain-rate components are assumed to act in series. The viscoelastic constitutive law corresponds to a Burgers model (Kelvin cell in series with a Maxwell component), and the plastic constitutive law corresponds to a Mohr–Coulomb model. The model used in this study is based on a classical viscoelastic constitutive law [34]. For the rock foundation, a viscoelastic, piecewise, and orthotropic constitutive model is assumed in the numerical analyses [37]. Furthermore, for the dam body concrete, a viscoelastic, homogeneous, and isotropic constitutive model is presumed in the earthquake analyses [37]. For the

(a)

(b)

(c)

FIGURE 2: General view of Ermenek arch dam: (a) downstream view, (b) aerial view, and (c) upstream view [33].
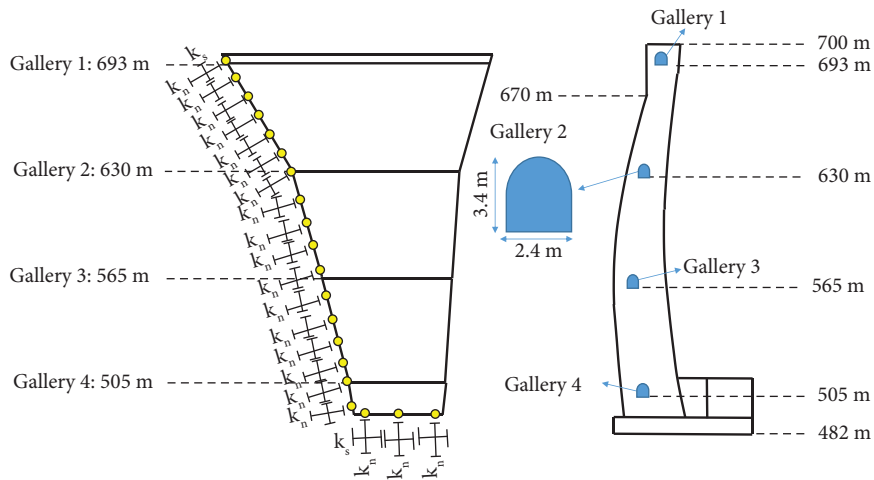

FIGURE 3: View of gallery spaces in the Ermenek arch dam body [33, 36].

creep analyses of the dam, fix reflecting BCs are defined to the dam boundaries in the x, y, and z directions. In this study, 18 various ground motions are used in the 3D nonlinear earthquake analyses of the Ermenek arch dam (Table 2). According to Table 2, it is seen that the earthquakes used in the analyses have different magnitudes and epicenter distances. In earthquake analyses, the X, Y, and Z components of each earthquake are used.

6. Earthquake Analysis Results of Ermenek Arch Dam

Examining the earthquake behavior of huge water structures such as arch dams is of great importance for the safety of these structures. Besides, due to climatic and seasonal changes, there may be constant differences in water levels in dams. This may negatively affect both the creep and
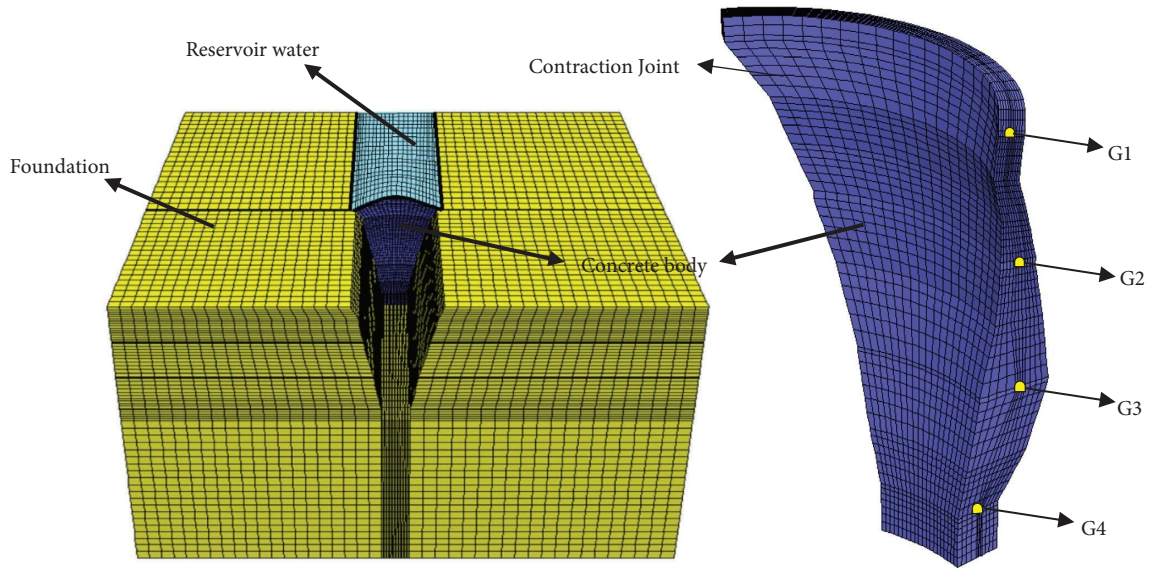
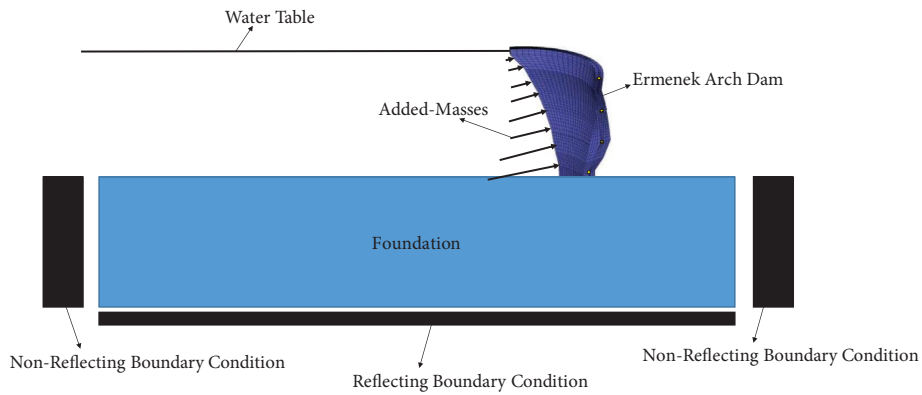Figure 4: 3D FD model of Ermenek arch dam.

Figure 5: View of water loads and water table.

Table 2: Characteristic properties of strong ground motions [35].

EQ	Earthquake	Year	Station	Mw	Duration (s)	d (km)	PGA	PGV	Ap/Vp	TPV	TP
1	Cape Mend.	1992	Rio Del OVP	7.1	40	18.5	0.39	44	8.7	1.3	1.2
2		1999	CHY028	7.6	40	7.3	0.82	67	12.1	0.9	0.8
3		1999	TCU060	7.6	40	9.5	0.20	36	5.45	11.0	8.4
4		1999	TCU087	7.6	40	3.2	0.13	41	3.11	8.0	9.5
5		1999	NSY	7.6	40	9.7	0.13	42	3.04	4.6	3.7
6	Chi-chi	1999	CHY101	7.6	40	11.1	0.44	115	3.75	4.8	4.7
7		1999	TCU063	7.6	40	10.4	0.13	73	1.75	3.4	5.2
8		1999	TCU059	7.6	40	17.8	0.17	59	2.83	6.5	6.0
9		1999	TCU057	7.6	40	12.6	0.09	43	2.05	7.5	6.6
10		1999	TCU101	7.6	40	2.9	0.2	68	2.89	8.5	7.6
11	Imp.val.	1979	El centro DA	6.5	40	5.3	0.35	71	4.84	2.6	4.5
12	Kobe	1995	KJM	6.9	20	0.6	0.60	74	7.95	0.8	1.4
13	Loma prieta	1989	Corralitos	6.9	40	5.1	0.48	45	10.46	0.8	0.7
14	N. palm spr.	1986	N.P.Spr. PO	6.0	20	8.2	0.59	73	7.93	1.1	1.4
15	Northrdg.	1994	Sly. Hosp.	6.7	20	6.4	0.84	130	6.34	1.6	1.9
16	Sup.hills	1987	PTS	6.6	20	0.7	0.45	112	3.94	1.9	2.2
17	Duzce	1999	Duzce	7.2	40	27	0.55	79	8.41	1.5	8.1
18	Kocaeli	1999	Izmit	7.6	40	6	0.63	86	9.46	1.6	8.4

earthquake behavior of these dams. For this reason, the earthquake behavior of the Ermenek arch dam, which was built for energy and irrigation purposes in Turkey, is investigated by considering different ground motions and various water levels in this study. After the 3D FD model of the dam is created, 18 different earthquake accelerations are effected on the base of the dam, and earthquake analysis results are obtained. Four various water heights selected for earthquake analyses are shown in detail in Table 3. In Table 3, it is seen that each water height is named with a different name. The time-dependent PS values in Figures 6–8 are obtained by considering the location of the maximum PS value in the dam body during the earthquake. Because the location of the maximum PS value occurring in the dam body is different for each earthquake analysis. In Figure 6, the PS results of the Ermenek arch dam are examined by considering different reservoir waters and 8 different ground motions. In all earthquake analyses, great increases are observed in the earthquake PS values occurring in the dam body as the reservoir water height increase. Moreover, it is concluded that the reservoir water height causes large PS concentrations around the gallery spaces. In Figure 6(a), the earthquake analysis results of the Ermenek dam are presented for the EQ1 earthquake. It is concluded that the PS values obtained on the dam body for C1 are higher than in other cases. This result reveals the effects of increases or decreases in hydrostatic pressure on the earthquake behavior of arch dams. During the EQ1 earthquake, the smallest PS values on the dam body are acquired in C3 and C4. For C1, important PS values are concentrated around gallery 4. This result shows how the changes in hydrostatic pressure values change the structural behavior of arch dams (Figure 6(a)). During the EQ2 earthquake, the maximum PS value gained for C1 is 7.88 MPa. In addition, for C2, C3, and C4, the highest stress values happening on the Ermenek dam body are 6.82 MPa, 3.29 MPa, and 1.82 MPa, respectively (Figure 6(b)). In Figure 6(c), the earthquake analysis results are presented for the EQ3 earthquake. When all cases are compared with each other, it is seen that the highest PS values on the dam body are obtained for C1. In addition, close PS values are observed on the dam body for C3 and C4 (Figure 6(c)). For C1 and C2, the largest PS values on the dam body are acquired around galley 2. For C3, the most critical stress values on the dam body took place around galley 4 (Figure 6(c)). During the EQ4 earthquake, 11.59 MPa maximum PS is observed on the dam body for C1 (Figure 6(d)). Moreover, the greatest PS values for C3, C4, and C5 are 10.82 MPa, 3.35 MPa, and 1.95 MP, respectively. For C3 and C4, the greatest stress concentrations are gotten at the base of the dam. When the earthquake PS on the dam body is assessed for the EQ5 earthquake, it can be seen that the maximum PS values on the dam body for C1 and C2 are close to each other (Figure 6(e)). Also, for C3 and C4, the greatest PS values on the dam body are 2.60 MPa and 1.43 MPa, respectively. According to Figure 6(f), it is seen that the largest PS values on the dam body for C1 occurred around gallery 3. Besides, the smallest stress values on the dam body are acquired for C4. During the EQ6 earthquake, the highest stress values on

the dam body for C2 and C3 are 2.66 MPa and 1.81 MPa, respectively (Figure 6(f)). In Figure 6(g), the earthquake behavior of the Ermenek dam is examined for the EQ7 earthquake. It is inferred that the stress values on the dam body for C3 and C4 are smaller than in C1 and C2. It is proposed that the reservoir water should be carefully modeled and acted on the dam while modeling arch dams and performing earthquake analyses. In Figure 6(h), the earthquake behavior of the Ermenek dam is examined for the EQ8 earthquake. For C1, the greatest PS value around gallery 4 is 8.86 MPa. Also, for C2 and C3, the highest stress values on the dam body took place around gallery 3. For C4, the greatest PS value observed on the concrete dam body is 1.09 MPa. For the EQ9 earthquake, it is observed that the maximum PS values for C1 and C2 are higher than C3 and C4 (In Figure 7(a)) It is deduced that gallery 4 is the most critical section of the Ermenek dam for the EQ9 earthquake. In Figure 7(b), the earthquake analysis results of the EQ10 earthquake are presented in detail. It is observed that the most critical PS values on the dam body occurred in C1 and C2. The highest stress values happening on the Ermenek dam for C3 and C4 are 2.71 MPa and 0.86 MPa, respectively. Moreover, for C3 and C4, the largest PS values on the dam body are gained at the base of the dam.

According to the EQ11 earthquake analysis results, it is observed that the maximum PS values for C1 are higher than the other cases (Figure 7(c)). It is inferred that the PS values on the dam body for C4 are lower than in C1. During the EQ12 earthquake, the greatest PS values on the dam body for C1 and C2 are 7.76 MPa and 6.18 MPa, respectively (Figure 7(d)). Furthermore, the most critical stress values on the dam body for C3 and C4 are concentrated around gallery 4. The earthquake analysis results for the EQ13 earthquake are presented in Figure 7(e). For C1, the greatest PS value happening in the Ermenek dam body is 11.89 MPa. The highest stress values on the dam body for C3 and C4 are 3.27 MPa and 1.49 MPa, respectively (Figure 7(e)). During the EQ14 earthquake, it is deduced that the highest principle stress values for C1 and C2 are greater than Case3 and C4 (Figure 7(f)). Besides, it is inferred that the most critical stress values for C1 and C2 are concentrated around the gallery 2. For C3 and C4, it is seen that the greatest PS values are concentrated at the base of the dam. During the EQ15 earthquake, the largest PS values on the dam body for C1 and C2 are 11.64 MPa and 11.05 MPa, respectively, and stress concentrations are observed around gallery 3 (Figure 7(g)). For the EQ16 earthquake, it is observed that the earthquake stress values for C1 and C2 are higher than C3 and C4 (Figure 7(h)). This result shows the effects of reservoir water height on the earthquake behavior of arch dams.

In Figure 8(a), time-dependent PS values observed on the Ermenek dam body during the EQ17 earthquake are presented in detail. According to Figure 8(a), the maximum PS value obtained for C1 is 9.07 MPa. In addition, the highest stress values on the dam body for C2, C3, and C4 are 9.96 MPa, 4.72 MPa, and 4.07 MPa, respectively. It is concluded that the PS values for C1 and C2 are close to each other and gallery 4 is the most critical section for the EQ17

TABLE 3: Reservoir water heights for earthquake analyses.

Case	Reservoir water height (m)
Case 1 (C1)	200
Case 2 (C2)	150
Case 3 (C3)	85
Case 4 (C4)	25

earthquake. In Figure 8(b), the PS values obtained on the dam body during the EQ18 earthquake are presented in detail. The greatest PS values occurring on the dam body for Case 1 and Case 4 are 11.18 MPa and 1.47 MPa, respectively. Besides, it is inferred that the stress values on the dam body for Case 2 are greater than the other cases. According to all earthquake analysis results, it is understood that reservoir water levels have great effects on the earthquake behavior of arch dams. It is observed that the earthquake stress values happening on the dam body for Case 1 (water level: 200 m) and Case 2 (water level: 150 m) are very close to each other. Moreover, it is concluded that the stress values on the dam body for C3 (water level: 85 m) are higher than in C4 (water level: 25 m). For C1 and C2, the largest PS values on the dam body are obtained around gallery 3 and gallery 4. In Figure 9, and 10, the earthquake displacement behavior of the Ermenek dam is examined by considering 18 different earthquakes. According to the earthquake analysis results, it is understood that different reservoir water levels changed the earthquake displacement behavior of the Ermenek dam visibly. Besides, various reservoir heights caused serious displacement changes around the gallery spaces of the Ermenek dam. In Figure 9(a), the maximum displacement values along the body height of the Ermenek dam are shown for the EQ1 earthquake. The maximum displacement value on the dam body is obtained for C1. In addition, smaller earthquake displacement values are observed for C4 as compared to other cases. For C1, serious displacements occurred around galleries 1, 2, 3, and 4 during the earthquake. Then, significant displacement changes are observed around galleries 2, 3, and 4 for C2. In C3, critical displacement values took place around galleries 3 and 4. It is clear from these results that significant earthquake displacement changes may occur around the gallery spaces of arch dams depending on the reservoir height during the earthquake. In Figure 9(b), the earthquake behavior of the Ermenek dam is assessed for the EQ2 earthquake. For C1, the largest earthquake displacement value obtained on the dam crest section during the earthquake is 73 mm. Furthermore, 44 mm and 29 mm maximum earthquake displacement values are observed on the dam crest for C3 and C4, respectively. For C2, significant earthquake displacement differences are acquired in galleries 2, 3, and 4. Then, significant displacements are observed around galleries 1, 2, 3, and 4 for C1 during the EQ2 earthquake. In Figure 9(c), the earthquake displacement results of the Ermenek dam are investigated by considering 4 various reservoir water levels. During the earthquake, 78 mm and 43 mm maximum earthquake displacements are obtained on the dam crest section for C1 and C4, respectively. Moreover, the maximum

displacement values on the dam crest for C2 are higher than in C3. For C1, 76 mm and 71 mm maximum earthquake displacements are observed in gallery 1 and gallery 2, respectively. In Figure 9(d), the earthquake displacement behavior of the dam is evaluated for the EQ4 earthquake. The maximum displacement values that occurred on the dam crest for C1 and C2 during the EQ4 earthquake are 62 mm and 57 mm, respectively (Figure 9(d)). In Figure 9(e), the maximum displacement values observed on the dam body are shown for the EQ5 earthquake. For C1, the maximum earthquake displacement values on the dam crest, galleries 1, 2, 3, and 4 are 86 mm, 89 mm, 80 mm, 67 mm, and 48 mm, respectively. Also, for Cases 2, 3, and 4, the largest displacement values on the dam crest are 83 mm, 66 mm, and 45 mm, respectively. These numerical results show the effects of changes in reservoir water levels on the earthquake displacement behavior of arch dams. Besides, significant displacement changes are observed around the gallery spaces depending on the reservoir water height. Figure 9(f) shows the maximum earthquake displacement values around the gallery spaces and crest section of the dam during the EQ6 earthquake. For Case 1, the earthquake displacement values observed on the dam crest are higher than in other sections of the dam. In addition, the largest displacement values on the dam crest section for C1 and C4 are 95 mm and 65 mm, respectively. During the EQ7 earthquake, for C1, the largest displacement values around gallery 1 and gallery 4 are 76 mm and 38 mm, respectively (Figure 9(g)). Then, the maximum earthquake displacement values in gallery 4 for Cases 2, 3, and 4 are 27 mm, 32 mm, and 15 mm, respectively. These results openly show that each reservoir water level has different earthquake displacement effects on gallery spaces of arch dams. It is deduced that the earthquake displacement values on the gallery increase as the height of water contacted by the dam body increases. In Figure 9(h), the earthquake displacement results occurring on the dam body during the EQ8 earthquake are presented in detail. According to numerical results, the largest earthquake displacement values on the dam crest section for C1 and C2 are 66 mm and 64 mm, respectively, and it is observed that the displacement values acquired along the dam body for C1 and C2 are close to each other. For C1, there are significant displacement differences around galleries 1, 2, 3, and 4. For C2, important earthquake displacement increases are observed around galleries 2, 3, and 4.

In Figure 10(a), the earthquake analysis results of the Ermenek dam are presented for the EQ9 earthquake. The maximum displacement values on the crest section for C1 and C2 are 57 mm and 55 mm, respectively. Besides, for C1, the maximum earthquake displacement values occurring around galleries 1, 2, 3, and 4 are 64 mm, 57 mm, 44 mm, and 29 mm, respectively. For C2, the largest displacement values taking place on the dam crest, galleries 1, 2, 3, and 4 are 54 mm, 49 mm, 42 mm, 33 mm, and 26 mm, respectively. Then, the largest displacement values on the dam body for Case 3 and Case 4 are observed to be smaller than Case 1 and Case 2. These results demonstrate the effects of reservoir water levels on the earthquake displacement behavior of arch dams (Figure 10(a)). The largest displacement values
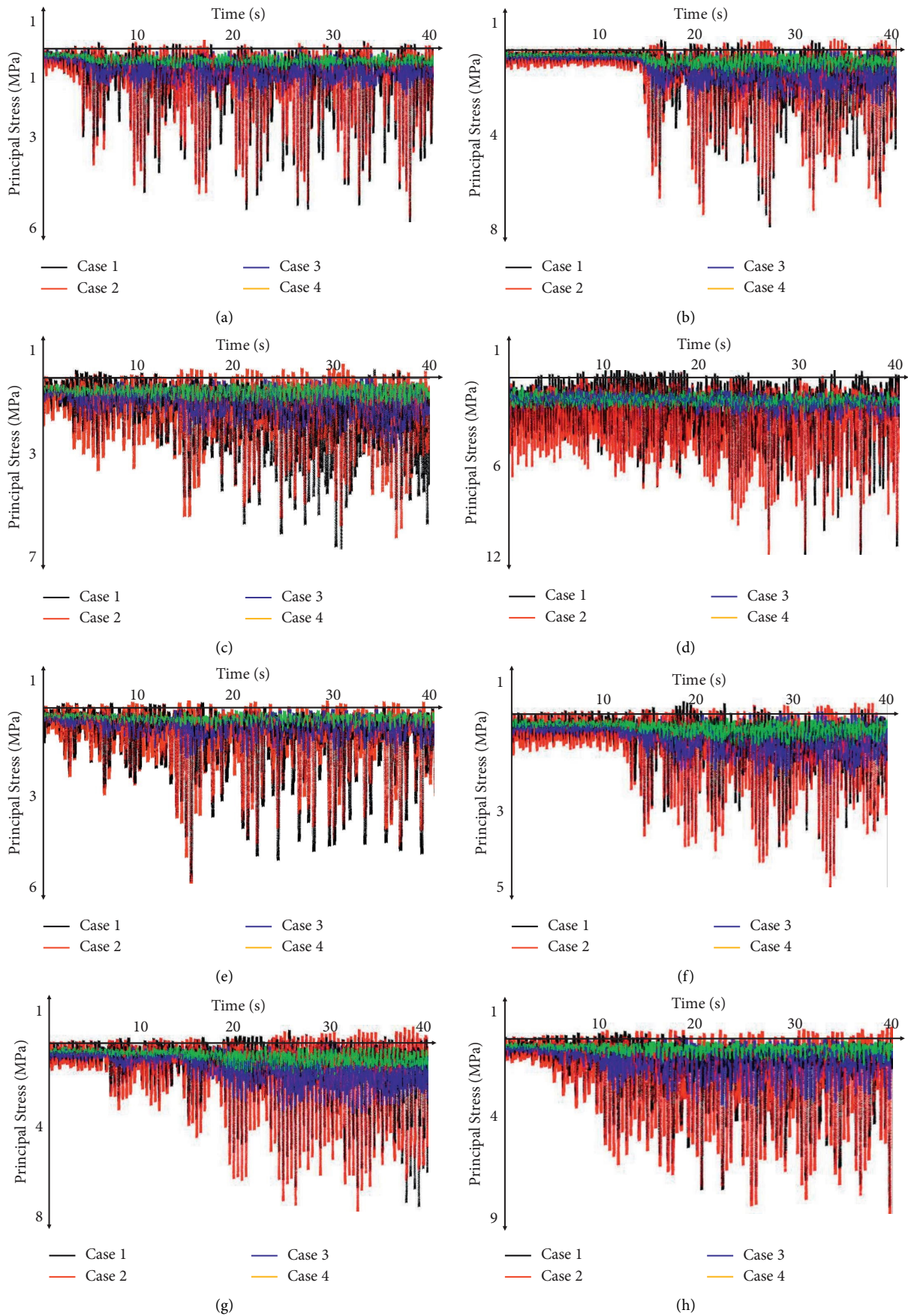
FIGURE 6: Earthquake PS results of Ermenek arch dam for EQ1–EQ8 earthquakes: (a) EQ1, (b) EQ2, (c) EQ3, (d) EQ4, (e) EQ5, (f) EQ6, (g) EQ7, and (h) EQ8.

(a)
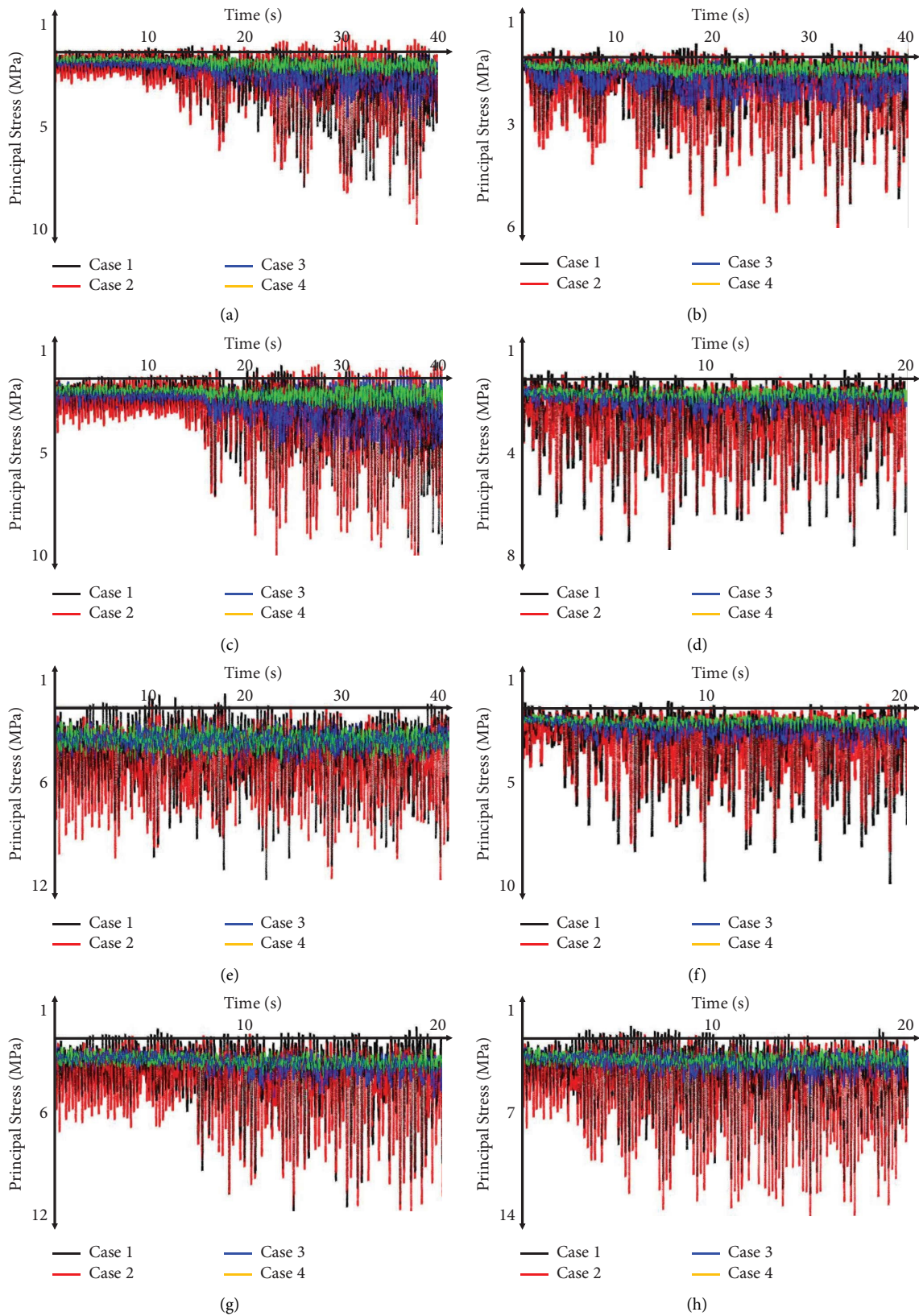

(b)

(c)

(d)

(e)

(f)

(g)

(h)

FIGURE 7: Earthquake PS results of Ermenek arch dam for EQ9–EQ16 earthquakes: (a) EQ9, (b) EQ10, (c) EQ11, (d) EQ12, (e) EQ13, (f) EQ14, (g) EQ15, and (h) EQ16.
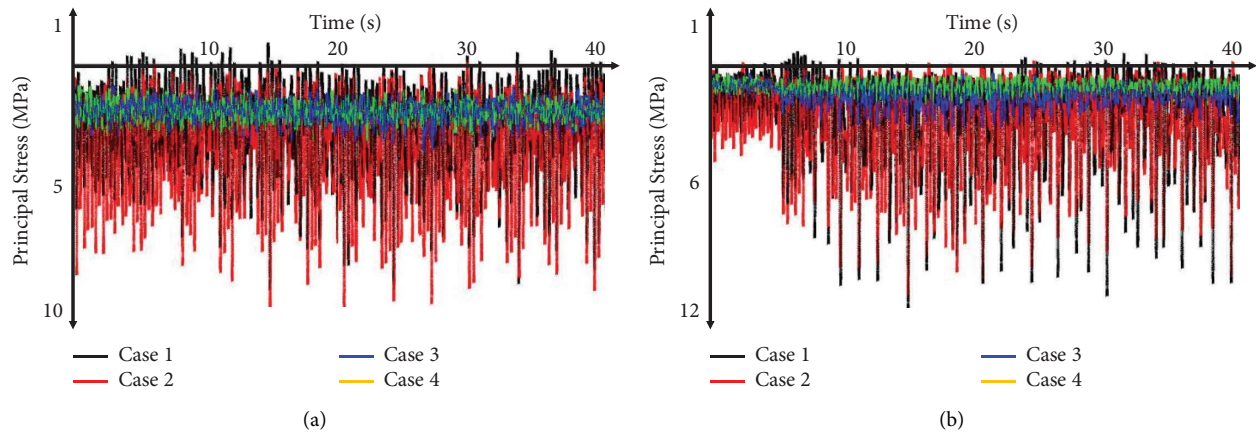
FIGURE 8: Earthquake PS results of Ermenek arch dam for EQ17-EQ18 earthquakes: (a) EQ17 and (b) EQ18.

observed on the dam body for the EQ10 earthquake are obtained for Case 1 (Figure 10(b)). Furthermore, when 4 different water heights are compared with each other, the smallest displacement values observed on the dam body happened in C4. In Figure 10(c), the earthquake analysis results are presented for the EQ11 earthquake. For C1 and C2, the largest displacement values occurring in the dam body are close to each other. The maximum displacement values obtained for C3 and C4 are smaller than for C2 and C1. For C1, the largest displacement values observed on the dam crest, galleries 1, 2, 3, and 4 are 82 mm, 84 mm, 72 mm, 64 mm, and 43 mm, respectively. Moreover, for C3, the maximum earthquake displacement values obtained on the crest, galleries 1, 2, 3, and 4 are 62 mm, 51 mm, 37 mm, 45 mm, and 29 mm, respectively. It is clear from these results that galleries 1, 2, 3, and 4 are the most critical sections for C1. For C2, the most important sections are galleries 2, 3, and 4. For C1, the largest earthquake displacement happening on the dam crest during the EQ12 earthquake is 63 mm (Figure 10(d)).

During the EQ13 earthquake, it is seen that the largest displacement values on the dam crest for C1 and C2 are 73 mm and 78 mm, respectively (Figure 11(a)). Moreover, as 4 various reservoir water levels are compared with each other, it is deduced that the smallest displacement values acquired on the dam crest took place in C4. According to 4 various earthquake analysis results, significant displacement differences are observed in 4 different gallery spaces (Figure 11(a)). In Figure 11(b), displacement values acquired along the dam body during the EQ14 earthquake are presented in detail. For Case 1, significant displacement differences are gained in galleries 1, 2, 3, and 4. Besides, the maximum displacement value occurring on the dam crest for Case 3 is higher than in Case 4. It is understood that when the height of water in contact with the dam body increases, the earthquake displacement values taking place on the gallery spaces and the dam body rise. These results show how important gallery spaces are for the earthquake behavior of arch dams (Figure 11(b)). During the EQ15 earthquake, the largest displacement happening on the dam crest for C1 is 64 mm. Furthermore, the largest earthquake displacement

values in gallery 1 for Cases 2, 3, and 4 are 58 mm, 46 mm, and 42 mm, respectively. For C3, significant displacement differences took place in galleries 3, 4, and, significant displacement values are observed around gallery 4 for C4 (Figure 11(c)). During the EQ16 earthquake, close earthquake displacement values are obtained on the dam body for C1 and C2 (Figure 11(d)). For the EQ17 earthquake, 57 mm and 58 mm maximum displacement values happened on the dam crest in C1 and C2, respectively. In C4, the largest displacements observed on the dam crest, galleries 1, 2, 3, and 4 are 36 mm, 34 mm, 24 mm, 16 mm, and 12 mm, respectively (Figure 11(e)). Moreover, during the EQ18 earthquake, the largest displacement values taking place on the dam crest for Case 1, Case 2, Case 3, and Case 4 are 83 mm, 76 mm, 58 mm, and 44 mm, respectively (Figure 11(f)). In Figures 12–17, the earthquake crack behaviors of the Ermenek arch dam are investigated for the full reservoir water. In addition, damage diagrams of the dam are calculated by comparing the maximum PS values occurring in the concrete body of the dam during the earthquake and the strength value of the concrete body of the dam. The damage diagrams of the dam are created by considering the total number of times the stress value occurring in the dam body during the earthquake exceeds the strength of the concrete body and the total number of stresses observed during the earthquake. While performing earthquake analyses in the FLAC3D program, a time step is defined for each earthquake. All definitions are performed using special fish functions. In FLAC3D, all stress values occurring in the dam body are automatically calculated during earthquake analysis. For example, if the duration of an earthquake is 40 seconds and the time step of the earthquake is 0.005, the program calculates a total of 8000 (40/0.005) stress values as a result of the earthquake analysis. These stress values can be output graphically with the help of special fish functions. In this study, all the stress values calculated on the dam body for each earthquake are transferred to the excel program. The compressive strength of the dam body is 30 MPa. Moreover, stress values exceeding 30 MPa (for example, 2000) are transferred to another excel program. As a result, the damage ratio (DR) value of a point on the dam body is
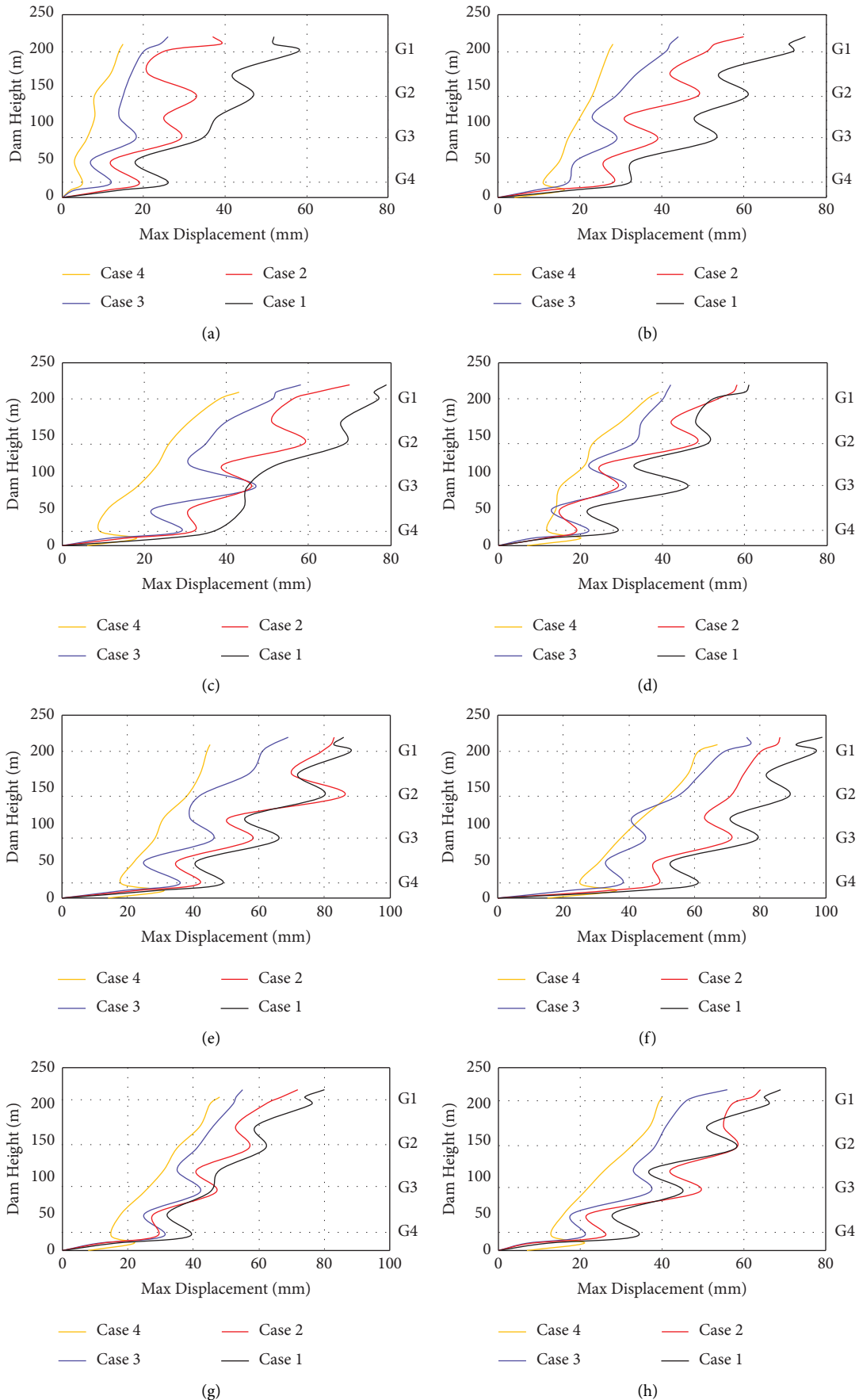
FIGURE 9: Earthquake displacement results of Ermenek arch dam for EQ1–EQ8 earthquakes: (a) EQ1, (b) EQ2, (c) EQ3, (d) EQ4, (e) EQ5, (f) EQ6, (g) EQ7, and (h) EQ8.
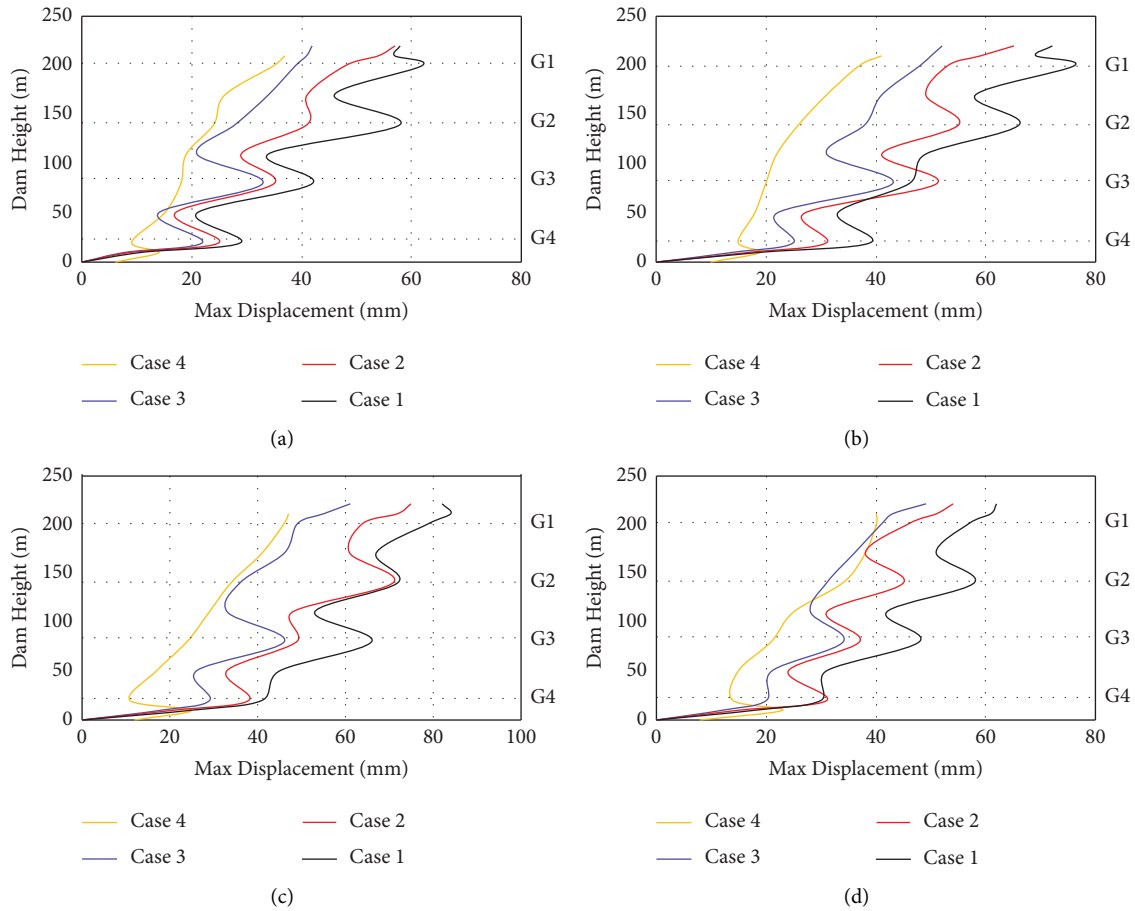
FIGURE 10: Earthquake displacement results of Ermenek arch dam for EQ9–EQ12 earthquakes: (a) EQ9, (b) EQ10, (c) EQ11, and (d) EQ12.

obtained by calculating 2000/8000. In other words, the DR value of the point on the dam body is 0.25 (25%). When the previous formulation is examined, the DRs are acquired by comparing the PS values obtained in the dam body during the earthquake period with the strength of the dam. The DRs of the Ermenek dam are calculated separately for each earthquake and analysis results are presented in detail in Figures 12–17. For the EQ1 earthquake, significant earthquake cracks are obtained in the dam body for each reservoir water level (Figure 12(a)). For C4, earthquake cracks occurred in the dam body around gallery 4. It is also concluded that for C3, cracks occurred around galleries 3 and 4 during the earthquake. Furthermore, for C2 and C1, it is observed that the earthquake crack values are concentrated around galleries 1, 2, 3, and 4 (Figure 12(a)).

In addition, it is deduced that for C4, the DR observed around gallery 4 is about 1, and the DR is very low around galleries 3, 2, and 1. For C3, significant DRs are observed around gallery 3 and gallery 4. According to the numerical results, critical DR values took place around galleries 1, 2, 3, and 4 for C1 and C2. It is concluded that as the reservoir water level rises, cracks and DR values around the gallery spaces of the arch dam increase (Figure 12(a)). During the EQ2 earthquake, significant earthquake cracks are observed around gallery 3 and gallery 4 for C4 (Figure 12(b)).

Moreover, similar cracks values occurred in the dam body for C1 and C2. This result shows that if the reservoir water level is 200 m and 150 m, similar damages may occur in the dam body. Besides, significant DR values are gained around gallery 3 and gallery 4 for C3 and C4. For C1 and C2, the DR ratios around galleries 1, 2, 3, and 4 are close to 1 (Figure 12(b)). During the EQ3 earthquake, critical cracks and DR values took place around the gallery spaces (Figure 12(c)). For C1 and C2, significant earthquake cracks values are observed in the dam body due to the various reservoir heights. In addition, as a result of the earthquake analysis results for C3 and C4, significant earthquake cracks took place only around gallery 3 and gallery 4. Considering the 4 different reservoir water levels, it is inferred that C1 and C2 are more critical for the earthquake crack behavior of Ermenek dam than the other cases. During the EQ3 earthquake, it is observed that the DR values calculated for C1 and C2 on the dam body and around the gallery spaces are approximately 1. This result shows that different reservoir water levels have various earthquake effects on the earthquake crack behavior of arch dams (Figure 12(c)). In Figure 13(a), the earthquake crack behavior of the Ermenek dam is examined for the EQ4 earthquake. As a result of the EQ4 earthquake, it is observed that the most critical earthquake cracks in the dam body occurred in C1 and C2.
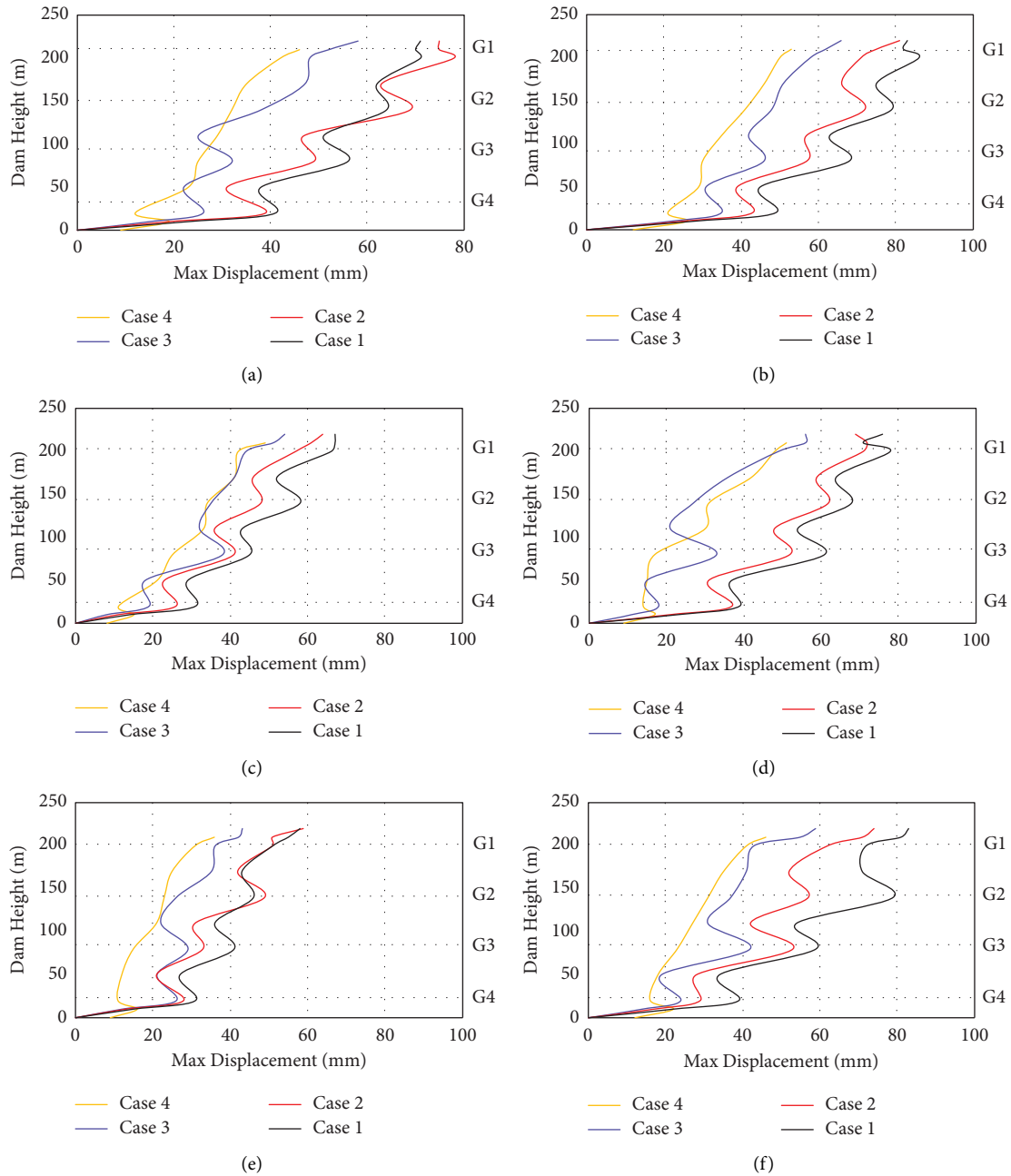
FIGURE 11: Earthquake displacement results of Ermenek arch dam for EQ13–EQ18 earthquakes: (a) EQ13, (b) EQ14, (c) EQ15, (d) EQ16, (e) EQ17, and (f) EQ18.

Moreover, significant earthquake cracks happened around gallery 3 and gallery 4 for C3 and C4. DR values for C1 and C2 are close to 1 (Figure 13(a)). It is deduced that earthquake cracks occurring in the dam body are similar to each other when the reservoir water level is 200 m and 150 m during the EQ5 earthquake (Figure 13(b)). Furthermore, the DRs calculated for C3 and C4 are smaller than for C1 and C2. The appearance of earthquake cracks observed in the Ermenek dam body during the EQ6 earthquake is shown in Figure 13(c). According to Figure 13(c), it is concluded that earthquake cracks in the dam body for C1 are more critical than in other cases. Besides, when 4 different reservoir water

levels are compared with each other, it is seen that the earthquake cracks observed in the dam body for C4 are less significant than in the other cases. During the EQ6 earthquake, for C1 and C2, the DRs on the dam body are between 0.5 and 1. Besides, for C3 and C4, it is understood that the DR obtained in the dam body is below 0.5. This result shows that the DR values of the Ermenek dam increase significantly as the reservoir water level that the arch dams body contacts increases.

In Figure 14(a), the earthquake crack and DR behavior of the Ermenek arch dam are examined for the EQ7 earthquake. In general, more severe earthquake cracks took
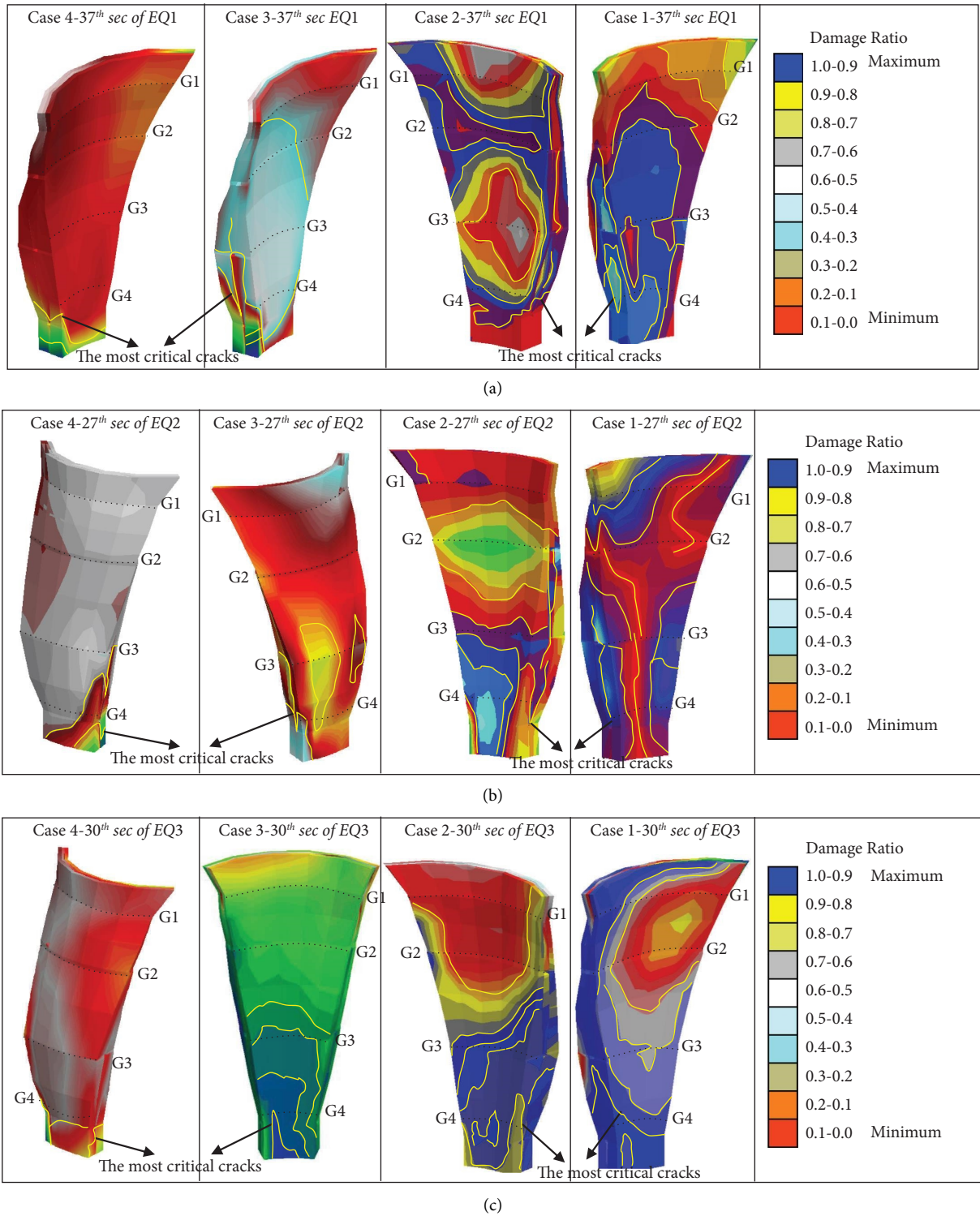
FIGURE 12: Earthquake crack performance of Ermenek arch dam for (a) EQ1 earthquake, (b) EQ2 earthquake, and (c) EQ3 earthquake.

place on the dam body for C1 as compared with other cases. Besides, similar earthquake cracks are acquired on the dam body for C3 and C4. DR values on the dam body for C1 are close to 1. For C2 and C3, the DR values on the dam body are between 0.5–0.7 (Figure 14(a)). During the EQ8 earthquake, it is concluded that serious cracks and DRs

occurred in the dam body for C1 and that no significant cracks are observed in the dam body for C4 (Figure 14(b)). In Figure 14(c), the earthquake analysis results of the Ermenek dam are presented for the EQ9 earthquake. Severe earthquake cracks are obtained for C1 around galleries 1, 2, 3, and 4. For C2 and C3, serious earthquake cracks are
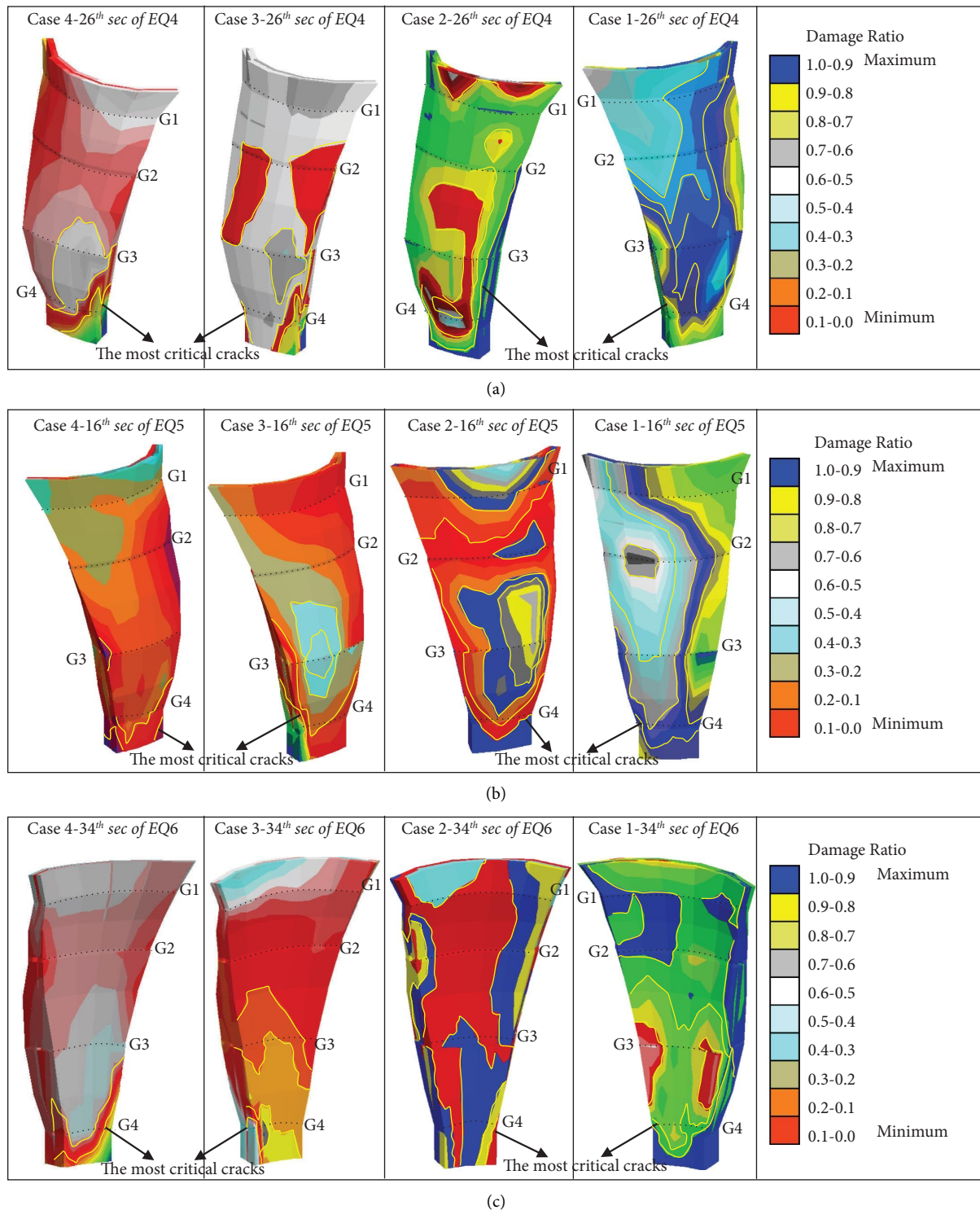
(a)

(b)

(c)

Figure 13: Earthquake crack performance of Ermenek arch dam for (a) EQ4 earthquake, (b) EQ5 earthquake, and (c) EQ6 earthquake.

observed around only gallery 4. The DR values on the dam body are between 0.7 and 1 for C1 and C2 (Figure 14(c)). During the EQ10 earthquake, more earthquake cracks are observed on the dam body for C1 than in the other cases (Figure 15(a)). During the EQ11 and EQ12 earthquakes, very important and critical earthquake cracks are gained on the dam body for C1. For C2, structural cracks are observed

around galleries 2, 3, and 4. It is clear from these results that serious cracks may occur in the dam body and around the gallery spaces if arch dams carry full capacity water load (Figures 15(b) and 15(c)). During the EQ13 earthquake, more critical cracks are obtained on the body of the Ermenek dam for C1 when compared to other cases. Also, significant earthquake cracks took place around galleries 2,
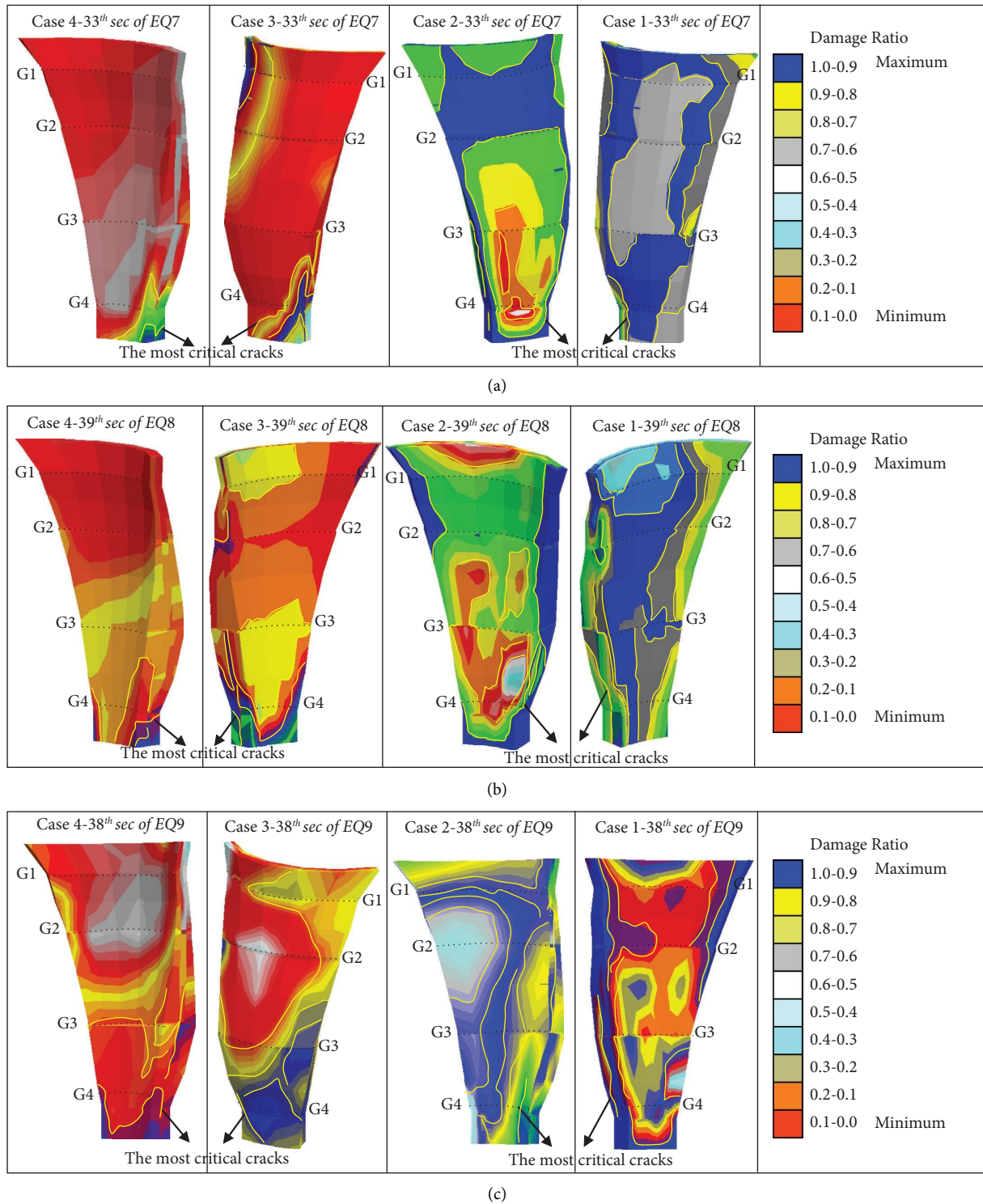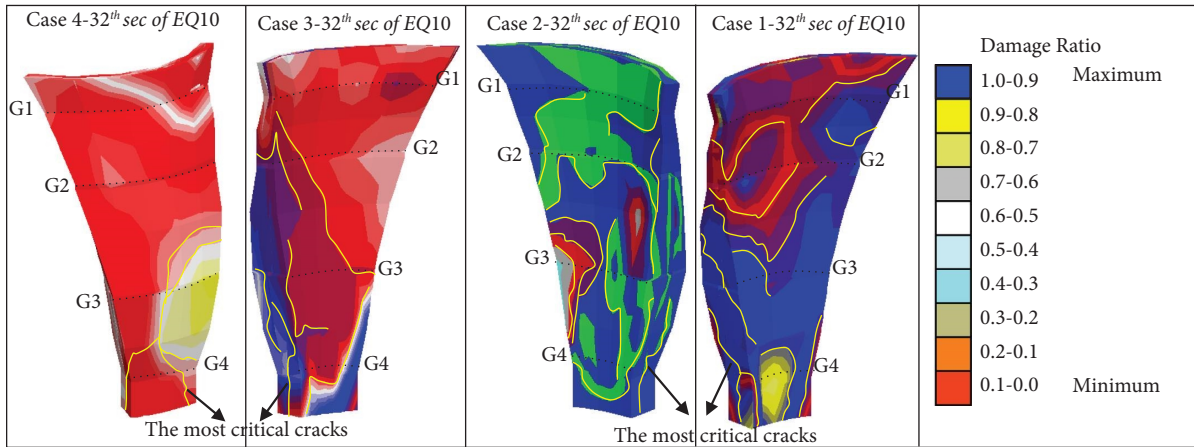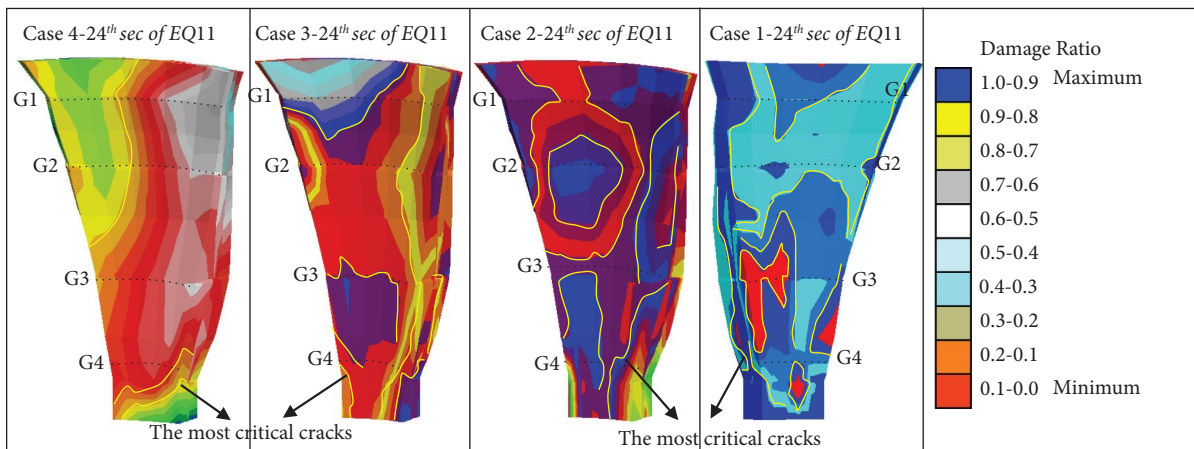
FIGURE 14: Earthquake crack performance of Ermenek arch dam for (a) EQ7 earthquake, (b) EQ8 earthquake, and (c) EQ9 earthquake.

3, and 4 for C2 and C3. For C1 and C2, the DR value on the dam body is generally above 0.7 (Figure 16(a)). During the EQ14 earthquake, the DR value for C1 is approximately 1 in the middle sections of the dam body. For C3, DR values around gallery 3 and gallery 4 are close to 1. These results show the effects of reservoir water levels on the earthquake behavior of arch dams and gallery spaces (Figure 16(b)).
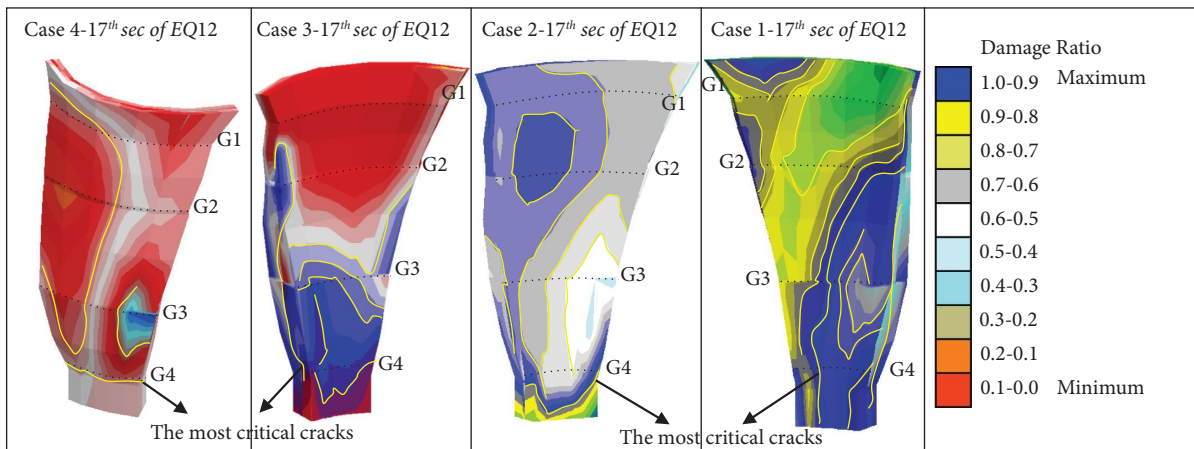
During the EQ15, EQ16, EQ17, and EQ18 earthquakes, significant earthquake cracks, and DR values are acquired for C1 and C2 in the body of the Ermenek dam. Earthquake cracks are generally concentrated around gallery spaces, and this result shows the researchers the effects of gallery spaces on the earthquake behavior of arch dams (Figures 16(c) and 17).

FIGURE 15: Earthquake crack performance of Ermenek arch dam for (a) EQ10 earthquake, (b) EQ11 earthquake, and (c) EQ12 earthquake.
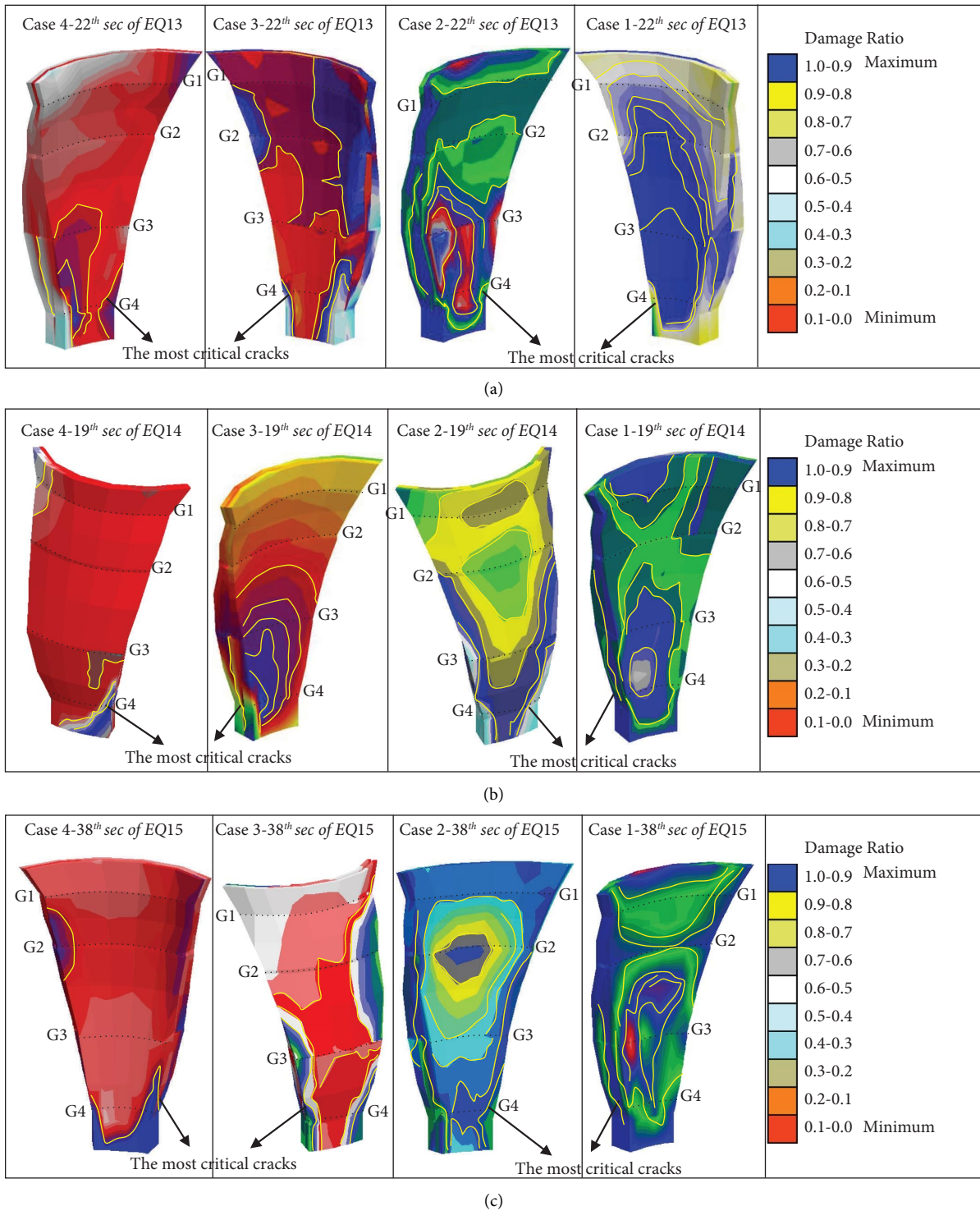
(a)

(b)

(c)

Figure 16: Earthquake crack performance of Ermenek arch dam for (a) EQ13 earthquake, (b) EQ14 earthquake, and (c) EQ15 earthquake.
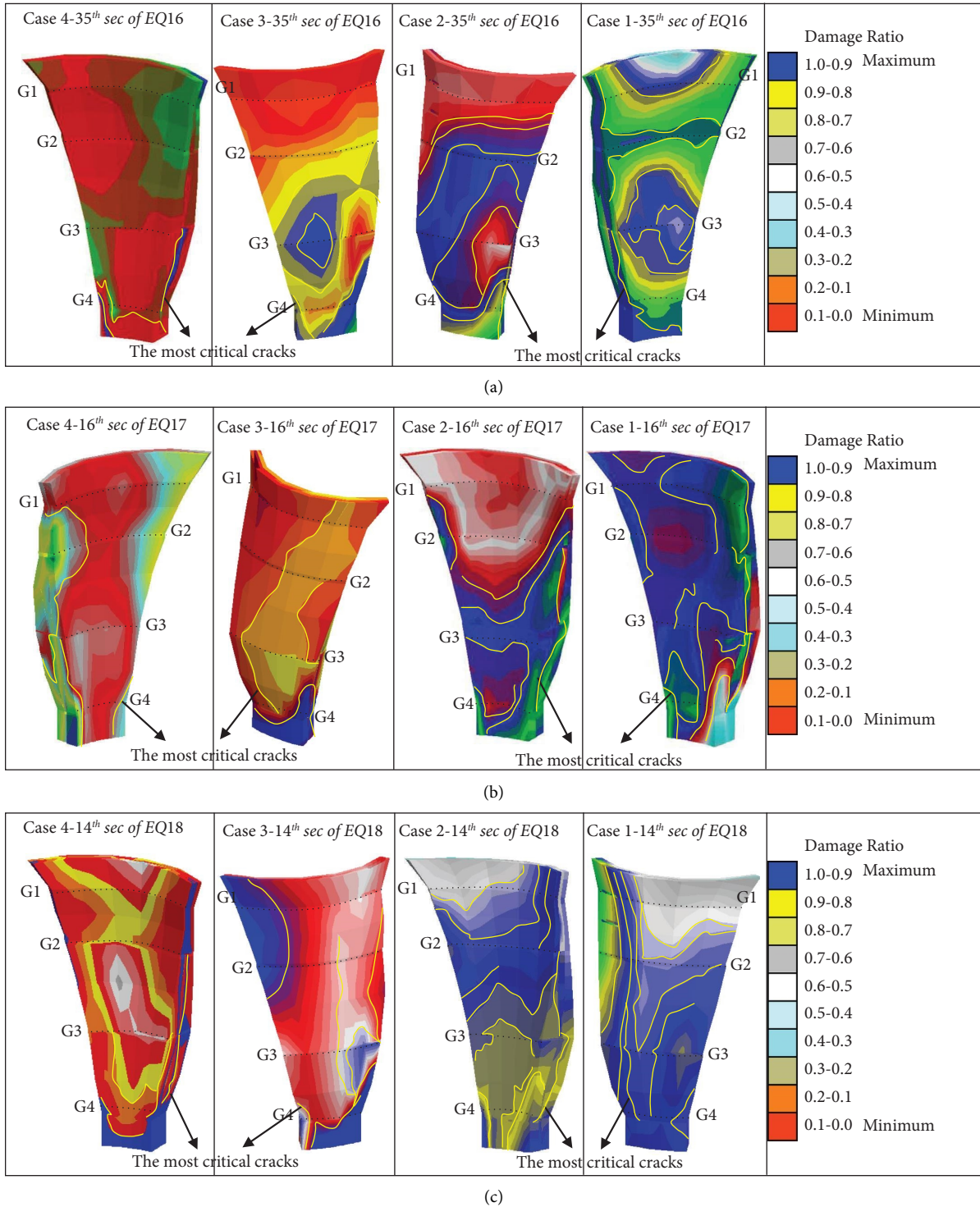
Figure 17: Earthquake crack performance of Ermenek arch dam for (a) EQ16 earthquake, (b) EQ17 earthquake, and (c) EQ18 earthquake.

7. Conclusions

Water is of great importance for the health and future of people. Special water structures are built to make optimum use of water, and one of the most important water structures is arch dams. Arch dams can safely carry high water forces in their body thanks to their special geometry and high body.

The amount of water in the bodies of arch dams constantly changes seasonally. In other words, these dams constantly carry different water loads in their bodies. For this reason, the effects of different water heights on the structural and earthquake behavior of arch dams should be consistently observed in detail. For this purpose, in this study, the earthquake behavior of the Ermenek arch dam, one of the

highest arch dams in Turkey, is investigated under different water heights (C1: 200 m, C2: 150 m, C3: 85 m, and C4: 25 m). First, the 3D FD model of the Ermenek dam is created according to the original dam project. The Burgers-Mohr material model is used for the concrete and foundation sections of the dam. Free-field and quiet nonreflecting BCs are defined to the boundaries of the dam model. While modeling the geometry of the dam, 4 different oval gallery spaces in the body of the dam are created following the dam project. For earthquake analyses, 18 different earthquakes are utilized and the following important results are obtained according to the analysis results.

(i) In the literature, the Burgers–Mohr material model used in this study has not been utilized for earthquake analyses of arch dams. This material model is a special model that is produced to model the creep behavior of both the concrete material of the dam and the foundation sections. Thanks to this model, time-dependent creep and earthquake behaviors of the arch concrete dam body are modeled and earthquake cracks in the dam body are revealed by considering the time-dependent creep behavior of concrete material. For this reason, this model used in this study provides important information to the literature in terms of examining the creep and earthquake analyses of arch dams and revealing concrete cracks.

(ii) Different water heights in the dam body have significantly changed the structural and earthquake behaviors of the Ermenek dam. According to the analysis results, it is concluded that different reservoir water levels create different earthquake stress and displacement values in the body of the arch dams. When the 4 different water heights used in the analyses are compared with each other, the largest PS and displacement values in the dam body are obtained for C1 (water level: 200 m). Besides, the smallest PS and displacement values in the dam body are observed for C4 (water level: 25 m). It is deduced that the stress and displacement values obtained in the dam body for C2 (water level: 150 m) are higher than in C3 (water level: 85 m).

(iii) It is observed that the earthquake crack values in the dam body for C1 and C2 are close to each other and larger than C3 and C4. Moreover, it is understood that the earthquake cracks in the dam body for C4 are smaller than in C3. These results showed that different reservoir water levels have significant effects on the earthquake crack behaviors of arch dams.

(iv) In this study, a new formulation has been proposed in the literature regarding the calculation of the DR of arch dams. This formulation is calculated by considering how many times the PS values occurring in the dam body over time exceed the bearing capacity of the dam concrete. It is seen that as the level of the reservoir water carried by the dam body rises, the DR rate in the dam body increases. When 4 different reservoir water levels are compared with each other, DRs in the range of 0.7–1 are observed in the dam body for C1 and C2. Furthermore, for C3 and C4, smaller DRs are obtained in the dam body as compared to C1 and C2. These results show that as the reservoir water level increases, the damage to the body of arch dams will increase.

(v) For C1, significant earthquake displacement values are obtained around galleries 1, 2, 3, and 4. Then, for C2, critical earthquake displacement values are observed around galleries 2, 3, and 4. For C3 and C4, significant displacement values occurred only around gallery 4. These results show that the earthquake displacement values around the gallery spaces vary depending on the reservoir water levels. In addition, it is concluded that gallery spaces are of great importance for the earthquake behaviors of arch dams and that gallery spaces should be carefully modeled while modeling or analyzing this dam type.

Data Availability

The data supporting the findings of the study are available from the corresponding author upon request.

Conflicts of Interest

The author declares that there are no conflicts of interest.

References

[1] M. T. Ahmadi, M. Izadinia, and H. Bachmann, "A discrete crack joint model for nonlinear dynamic analysis of concrete arch dam," *Computers & Structures*, vol. 79, no. 4, pp. 403–420, 2001.

[2] M. Akkose, A. Bayraktar, and A. A. Dumanoglu, "Reservoir water level effects on nonlinear dynamic response of arch dams," *Journal of Fluids and Structures*, vol. 24, no. 3, pp. 418–435, 2008.

[3] T. B. Amina, B. Mohamed, L. André, and B. Abdelmalek, "Fluid–structure interaction of Brezina arch dam: 3D modal analysis," *Engineering Structures*, vol. 84, pp. 19–28, 2015.

[4] J. Feng, H. Wei, J. Pan, Y. Jian, J. Wang, and C. Zhang, "Comparative study procedure for the safety evaluation of high arch dams," *Computers and Geotechnics*, vol. 38, no. 3, pp. 306–317, 2011.

[5] A.-Y. Jin, J.-W. Pan, J.-T. Wang, and C. Zhang, "Effect of foundation models on seismic response of arch dams," *Engineering Structures*, vol. 188, pp. 578–590, 2019.

[6] H. Li, G. Wang, B. Wei, Y. Zhong, and L. Zhan, "Dynamic inversion method for the material parameters of a high arch dam and its foundation," *Applied Mathematical Modelling*, vol. 71, pp. 60–76, 2019.

[7] V. Lotfi and R. Espandar, "Seismic analysis of concrete arch dams by combined discrete crack and non-orthogonal smeared crack technique," *Engineering Structures*, vol. 26, no. 1, pp. 27–37, 2004.

[8] V. Lotfi, "Direct frequency domain analysis of concrete arch dams based on FE-(FE-HE)-BE technique," *Computers and Concrete*, vol. 1, no. 3, pp. 285–302, 2004.

[9] T. Ma, Z. Feng, C. Tang, P. Lin, and K. P. Yadav, "Overall stability analysis of xiluodu high arch dam based on fine three-dimension numerical modeling," *Advances in Civil Engineering*, vol. 2021, Article ID 6641974, 15 pages, 2021.

[10] S. Malla and M. Wieland, "Analysis of an arch–gravity dam with a horizontal crack," *Computers & Structures*, vol. 72, no. 1-3, pp. 267–278, 1999.

[11] H. Mirzabozorg, M. Varmazyari, and S. A. Gharehbaghi, "Seismic evaluation of existing arch dams and massed foundation effects," *Soils and Foundations*, vol. 56, no. 1, pp. 19–32, 2016.

[12] A. J. Moradloo, A. Adib, and A. Pirooznia, "Damage analysis of arch concrete dams subjected to underwater explosion," *Applied Mathematical Modelling*, vol. 75, pp. 709–734, 2019.

[13] J. Nasserzare, Y. Lei, and S. Eskandari-Shiri, "Computation of natural frequencies and mode shapes of arch dams as an inverse problem," *Advances in Engineering Software*, vol. 31, no. 11, pp. 827–836, 2000.

[14] H. Li, S. Fu, G. Li, and G. Hu, "FEA of effects induced by diurnal temperature variation on downstream surface of xiaowan arch dam," *Advances in Civil Engineering*, vol. 2021, Article ID 6300387, 11 pages, 2021.

[15] Q. Xu, S. Xu, J. Chen, and J. Li, "Investigation of stochastic seismic response and index correlation of an arch dam using endurance time analysis method," *Advances in Civil Engineering*, vol. 2020, Article ID 8862869, 23 pages, 2020.

[16] X. Pan, G. Wang, W. Lu, P. Yan, M. Chen, and Z. Gao, "The effects of initial stresses on nonlinear dynamic response of high arch dams subjected to far-field underwater explosion," *Engineering Structures*, vol. 256, Article ID 114040, 2022.

[17] S. Pereira, F. Magalhães, J. P. Gomes, Á. Cunha, and J. V. Lemos, "Dynamic monitoring of a concrete arch dam during the first filling of the reservoir," *Engineering Structures*, vol. 174, pp. 548–560, 2018.

[18] A. Aftabi Sani and V. Lotfi, "Dynamic analysis of concrete arch dams by ideal-coupled modal approach," *Engineering Structures*, vol. 32, no. 5, pp. 1377–1383, 2010.

[19] A. C. Singhal and M. S. Zuroff, "Dynamic analysis of dams with nonlinear slipjoints," *Soil Dynamics and Earthquake Engineering*, vol. 17, no. 3, pp. 185–196, 1998.

[20] S. Li, L. Ding, L. Zhao, and W. Zhou, "Optimization design of arch dam shape with modified complex method," *Advances in Engineering Software*, vol. 40, no. 9, pp. 804–808, 2009.

[21] T. Szczesiak, B. Weber, and H. Bachmann, "Nonuniform earthquake input for arch dam–foundation interaction," *Soil Dynamics and Earthquake Engineering*, vol. 18, no. 7, pp. 487–493, 1999.

[22] P. Wei, P. Lin, H. Peng, Z. Yang, and Y. Qiao, "Analysis of cracking mechanism of concrete galleries in a super high arch dam," *Engineering Structures*, vol. 248, Article ID 113227, 2021.

[23] J.-T. Wang, D.-D. Lv, F. Jin, and C.-H. Zhang, "Earthquake damage analysis of arch dams considering dam–water–foundation interaction," *Soil Dynamics and Earthquake Engineering*, vol. 49, pp. 64–74, 2013.

[24] R.-k. Wang, L. Chen, and C. Zhang, "Seismic design of Xiluodu ultra-high arch dam," *Water Science and Engineering*, vol. 11, no. 4, pp. 288–301, 2018.

[25] J.-T. Wang, M.-X. Zhang, A.-Y. Jin, and C.-H. Zhang, "Seismic fragility of arch dams based on damage analysis," *Soil Dynamics and Earthquake Engineering*, vol. 109, pp. 58–68, 2018.

[26] B. Wu, J. Niu, H. Su, M. Yang, Z. Wu, and X. Cui, "An approach for deformation modulus mechanism of super-high arch dams," *Structural Engineering & Mechanics*, vol. 69, no. 5, pp. 557–566, 2019.

[27] X. Xue, X. Yang, and W. Zhang, "Damage analysis of arch dam under blast loading," *Computers and Concrete*, vol. 12, no. 1, pp. 65–77, 2013.

[28] X. Xue and X. Yang, "Earthquake safety assessment of an arch dam using an anisotropic damage model for mass concrete," *Computers and Concrete*, vol. 13, no. 5, pp. 633–648, 2014.

[29] Q. Yang, Y. Liu, Y. Chen, and W. Zhou, "Stability and re-inforcement analyses of high arch dams by considering deformation effects," *Journal of Rock Mechanics and Geotechnical Engineering*, vol. 2, no. 4, pp. 305–313, 2010.

[30] X. Yu, Y. F. Zhou, and S. Z. Peng, "Stability analyses of dam abutments by 3D elasto-plasticfinite-element method: a case study of Houhe gravity-arch dam in China," *International Journal of Rock Mechanics and Mining Sciences*, vol. 42, no. 3, pp. 415–430, 2005.

[31] Q.-L. Zhang, D.-Y. Li, F. Wang, and B. Li, "Numerical simulation of nonlinear structural responses of an arch dam to an underwater explosion," *Engineering Failure Analysis*, vol. 91, pp. 72–91, 2018.

[32] Q. Xu, T. Zhang, J. Chen, J. Li, and C. Li, "The influence of reinforcement strengthening on seismic response and index correlation for high arch dams by endurance time analysis method," *Structures*, vol. 32, pp. 355–379, 2021.

[33] Dsi, *General Directorate of State Hydraulic Works*, DSI, Ankara, Turkey, 2022.

[34] Itasca, *Inc. FLAC Version 5 User Manual*, Itasca Consulting Group Inc, Minneapolis, USA, 2002.

[35] Peer, "PEER ground motion database - PEER center," 2022, https://ngawest2.berkeley.edu/spectras/new?sourceDb_flag=1.

[36] S. Alcay, C. O. Yigit, C. Inal, and A. Ceylan, "Analysis of displacement response of the Ermenek dam monitored by an integrated geodetic and pendulum system," *International Journal of Civil Engineering*, vol. 16, no. 10, pp. 1279–1291, 2018.

[37] M. Colombo, M. Domaneschi, A. Ghisi et al., "Stress verifications of large concrete existing dams: comparison of two seismic Italian codes," *International Journal of Earthquake Engineering*, vol. 34, no. 1, pp. 61–81, 2017.

[38] M. Colombo, M. Domaneschi, and A. Ghisi, "Existing concrete dams: loads definition and finite element models validation," *Structural Monitoring and Maintenance*, vol. 3, no. 2, pp. 129–144, 2016.

[39] M. Colombo, M. Domaneschi, A. Ghisi, and S. Griffini, "Bearable maximum seismic action for existing concrete dams by Italian standard," *International Journal of Earthquake Engineering*, vol. 35, no. 1, pp. 3–24, 2018.

[40] M. Karalar and M. Çavuşli, "Effect of normal and shear interaction stiffnesses on three-dimensional viscoplastic creep behaviour of a CFR dam," *Advances in Civil Engineering*, vol. 2018, Article ID 2491652, 17 pages, 2018.